Progress In Electromagnetics Research, PIER 92, 235–253, 2009

HIGH-ORDER ELECTROMAGNETIC MODELING OF SHORTWAVE INDUCTIVE DIATHERMY EFFECTS

M. Parise and S. Cristina

University Campus Bio-Medico of Rome
Via Alvaro del Portillo 21, Rome 00128, Italy

Abstract—A high-order closed-form solution for the specific absorption rate (SAR) distribution induced inside a plane geometry fatmuscle tissue by a shortwave diathermy induction coil is presented. The solution is derived starting from the complete integral expressions for the electromagnetic field components generated by a currentcarrying circular loop located horizontally above a stratified earth. It is valid in a wide frequency range, and is flexible to any multi-turn coil configuration. The spatial distribution of the SAR induced in the muscle tissue by a flat round coil is computed by using the proposed formulation, the zero-order quasi-static one, and the finite difference time domain (FDTD) method. Excellent agreement is demonstrated to exist between the results provided by the new approach and those achieved through FDTD simulations. On the contrary, the performed computations show that the zero-order solution leads to over-estimate the SAR. The performances of the round and figure-eight coil geometries are compared. Despite of what has been argued in previously published papers, it turns out that the figure-eight coil is less energetically efficient than the round one. The work in the present paper is an extension of a previous work.

1. INTRODUCTION

Shortwave or Radio Frequency (RF) inductive diathermy therapy consists of using an applicator coil fed by a radiofrequency generator to produce electric currents and ohmic heating in subcutaneous fat and muscle tissues by electromagnetic induction. This widespread electrotherapy treatment modality is employed for multiple purposes, that is to accelerate wound healing and nerve regeneration, to deal with

Corresponding author: M. Parise (m.parise@unicampus.it).

vascular occlusion, and to reduce post-surgery pain or relieve muscle spasms [1–3]. In particular, recent studies about wound healing [1] proved that the application of shortwave diathermy enhances the proliferation rates of the fibroblast cells, which are involved in the synthesis of collagen and contribute to repair scar tissues. Previously, several tests performed on patients with peripheral vascular desease (PVD) [2] pointed out how the production of heating in deep tissues causes vasodilation of the local vessels, thus increasing the blood flow. Moreover, heat produced by applicator coils is used in combination with conventional radiotherapy and chemotherapy for the management of tumors (loco-regional hyperthermia [4–8]).

Regardless of the therapeutic purpose, diathermy treatment planning necessitates the a priori knowledge of the Specific Absorption Rate (SAR) patterns induced in human tissues by coils.

When, as frequently occurs, the illuminated structure is human back or abdomen, the SAR can be computed assuming a planar tissue geometry, provided both the coil-to-subject spacing and coil radius are small if compared to the characteristic dimension of the cross section of the body trunk [3, 9, 10]. The EM analysis can then be efficiently performed through analytical techniques, which require computer resources and computation times significantly smaller than those implied by numerical procedures, and are suitable for the comparative evaluation of various exposure conditions and coil configurations. Closed-form expressions for the heating patterns generated in simplified tissue models (semi-infinite plane and cylinder) by circular coils were derived under the quasi-static field assumption [3, 10–13], that is neglecting the high-frequency effects due to the displacement current (in both the air and the tissue) and the depth of penetration (in the tissue). Yet, at the most commonly used diathermy frequencies of 27.12 MHz or 40.68 MHz, any quasi-static (i.e., zero-order) model fails because the depth of penetration in muscle tissue is smaller than the thickness of the layer, and more complex formulations are required in order to achieve accurate results.

The aim of this paper is to present a refined high-order model of the planar fat-muscle tissue combination exposed to radio waves from a diathermy coil, that responds to the following two requirements. First, it must be valid in the quasi-static as well as the nonquasi-static frequency regions (i.e., up to the maximum diathermy operating frequency). Second, it has to allow the analytical close-formulation for the SAR distribution generated by any feasible flat multi-turn geometry. The latter requirement ensures minimum time consumption when it is required to optimize the coil to produce a desired heating pattern. The proposed model is based on the exact integral

representation for the electric field produced by a circular turn placed above a stratified medium [14]. At first, such field integral is cast into a form suitable for the application of the Cauchy's residue theorem. Next the non-oscillating part of the integrand is accurately approximated with a rational function according to the fitting algorithm [15], and finally the residue theorem is applied providing a closed-form expression for the radial distribution of the electric field at any plane parallel to the air-tissue boundary. The process of integration takes only few seconds, since the computational effort is limited to the extraction of the poles and residues that describe the rational approximation. The heating patterns produced by multi-turn coils are computed by superposing the contributions arising from the different turns. Moreover, since the function to be approximated is unique for all the possible turns at a given height from the medium, a single run of the fitting algorithm is enough to achieve the performances of an infinite number of flat coils of various shapes and sizes. This feature brings down the computational cost of any iterative process aimed at optimizing the coil geometry, and makes the proposed model and computation methodology advantageous over standard purely numerical techniques used to solve electromagnetic boundary value problems, like the FDTD and finite element methods.

The SAR distribution produced by the round coil in the region occupied by muscle tissue is computed by applying the proposed approach. The obtained results closely agree with the corresponding ones provided by FDTD simulations, while match the data achieved with the quasi-static formulation only in the low frequency range. At higher frequencies (like the diathermy operating frequencies) the quasi-static model leads to over-estimate the maximum SAR up to about 30%.

Furthermore, to illustrate the flexibility of the developed method to deal with different coil configurations, the poles and residues that have been obtained for the case of a round coil are also used to investigate the heating pattern of a figure-eight (or butterfly) geometry made up of a coplanar pair of coils with their perimeters touching. It is confirmed that this configuration produces, with respect to the single round coil, a more focused field under the joint, as was also concluded in previous papers [10, 11]. What has not yet been pointed out, and instead emerges from the present analysis, is that, surprisingly, using a figure-eight applicator worsens the efficiency of the system.

The present article is an extension of a previous conference paper [16]. It exhibits a more elegant and simplified theoretical development, which allows to reduce from two to one the number of rational approximations to be calculated. As a result, the

computational time is halved as well. Furthermore, unlike the preceding formulation, the solution proposed here can be easily adjusted to any coil shape. Finally, a large number of numerical results are presented and investigated in this extended version.

2. THEORY

Consider a single-turn circular coil carrying a time-varying current placed horizontally above a planar skin-fat-muscle tissue combination, as shown in Fig. 1. The geometric configuration is symmetric with respect to the coil axis, and a cylindrical coordinate system (r, φ, z) is suitably introduced and fixed on the skin surface.

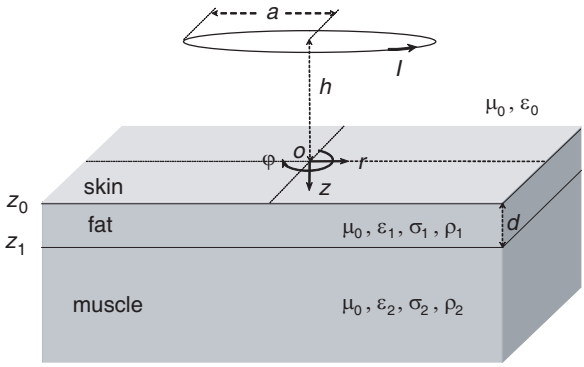

Figure 1. Geometry and coordinates for a skin-fat-muscle planar tissue exposed to a diathermy induction circular loop.

The thickness of the region occupied by the skin is negligible if compared to those of fat and muscle layers, to the local wavelength and plane wave depth of penetration, and the EM field arising from the corresponding induced currents can be ignored. The thickness of the fat layer is d, while the muscle tissue can be considered a semi-infinite medium as long as its thickness is greater than the depth of penetration. The dielectric permittivity, electric conductivity, and mass density are respectively ϵ_1, σ_1, and ρ_1 for fat, ϵ_2, σ_2, and ρ_2 for muscle. The combination is assumed to have the magnetic permeability of free space μ_0. The coil, with radius a, is situated in free space at height h from air-tissue interface, and carries a current equal to $Ie^{j\omega t}$. Because of symmetry about the z-axis, the electric field generated by the loop has no vertical component, and the EM field is transverse electric (TE). The time-harmonic factor $e^{j\omega t}$ is suppressed throughout analysis. The exact integral representation for the nonzero electric field

component induced in the tissue is given by [14]:

$$\overline{E}_{\varphi}(r,z) = \frac{2\overline{I}a}{\pi}\int_0^{\infty} f(\lambda,z)J_1(\lambda a)J_1(\lambda r)\,\lambda d\lambda, \tag{1}$$

with

$$f(\lambda,z) = \begin{cases} g(\lambda)\left[e^{-u_1(z-d)} + R_1^{TE}e^{u_1(z-d)}\right], & 0 < z < d, \\ g(\lambda)\left(1+R_1^{TE}\right)e^{-u_2(z-d)}, & z > d, \end{cases} \tag{2}$$

$$g(\lambda) = \frac{\pi\omega\mu_0(1+R_0^{TE})e^{-u_0 h}}{4ju_0\left(e^{u_1 d} + R_1^{TE}e^{-u_1 d}\right)}, \tag{3}$$

and being

$$u_m = \left(\lambda^2 - \omega^2\mu_m\epsilon_m + j\omega\mu_m\sigma_m\right)^{\frac{1}{2}}, \tag{4}$$

$$R_0^{TE} = \frac{u_0\left[u_1 + u_2\tanh\left(u_1 d\right)\right] - u_1\left[u_2 + u_1\tanh\left(u_1 d\right)\right]}{u_0\left[u_1 + u_2\tanh\left(u_1 d\right)\right] + u_1\left[u_2 + u_1\tanh\left(u_1 d\right)\right]}, \tag{5}$$

$$R_1^{TE} = \frac{u_1 - u_2}{u_1 + u_2}, \tag{6}$$

respectively, the propagation coefficient in the m-th layer and the transverse electric plane wave reflection coefficients at $z = 0$ and $z = d$.

The integral on the right-hand side of (1) is a first-order Hankel transform. In principle, digital linear filter technique [17, 18] based on exponential sampling would be suitable for the evaluation of this transform, as the kernel function is seen to decay exponentially when the absolute value of λ increases. Yet, it is known that the conventional approach to digital filter design relies on repeated usage of the sample domain Wiener-Hopf least-squares method within an optimization loop [18]. Since the computational cost of the Wiener-Hopf method is proportional to the square of the filter length, such multiple executions can take a huge amount of time for very long filter designs [17]. Thus, the accuracy of the result of computation can be theoretically enhanced by increasing the filter length, but at the cost of running an expensive optimization process. Furthermore, any digital filter is optimized for a specific known integral transform (the so-called test function), and may lead to uncertain results when applied to the calculation of different transforms.

In order to overcome the intrinsic limitations of the digital filter technique, a new method is proposed for carrying out the evaluation of the integral on the right-hand side of (1). The key feature of the method is that integration is performed analytically by applying the

Cauchy's residue theorem, once the function (2) is replaced with an accurate rational approximation. At first the integral is cast into a form in which the range of integration extends from $-\infty$ to ∞. Proceeding as discussed in [19] allows to derive the following representation for $\overline{E}_\varphi(r,z)$ alternative to (1):

$$\overline{E}_\varphi(r,z) = \frac{\overline{I}a}{\pi} \int_{C_1} f\,(\lambda,z)\, q(\lambda,r)\lambda\, d\lambda \tag{7}$$

with

$$q\,(\lambda,r) = \begin{cases} H_1^{(1)}(\lambda a)J_1(\lambda r), & r < a, \\ J_1(\lambda a)H_1^{(1)}(\lambda r), & r > a, \end{cases} \tag{8}$$

and being $H_1^{(1)}(\xi)$ the first-order Hankel function of the first kind.

The contour of integration C_1 extends along the upper shore of the negative real λ-axis (the branch cut of the Hankel function $H_1^{(1)}$) and the positive real λ-axis on the complex λ-plane, as shown in Fig. 2. It should be noted that, when increasing $|\lambda|$, the function $f(\lambda,z)$ rapidly decay in all the quadrants of the complex λ-plane, while the function $q\,(\lambda,r)$ exponentially diverges or decays depending on whether $\mathrm{Im}[\lambda]<0$ or $\mathrm{Im}[\lambda]>0$. Hence, in agreement with Jordan's lemma [20], Equation (7) does not suffer any alteration when closing the contour C_1 with an infinite semicircle about the upper-half of the complex λ-plane. It reads:

$$\overline{E}_\varphi(r,z) = \frac{\overline{I}a}{\pi} \int_{C_1+C_2} f\,(\lambda,z)\, q(\lambda,r)\lambda\, d\lambda, \tag{9}$$

being C_2 the semicircle at infinity (a dashed line in Fig. 2).

As proved in [20], any integral along a closed path C can be evaluated by means of the residue theorem, provided the integrand is analytic inside and on C except for a number of pole singularities. In the present case, the square-root terms (4) introduce branch point singularities all over the complex λ-plane, which prevent from applying the residue theorem. To eliminate such branch points, the rational approximation

$$f\,(\lambda,z) \cong \sum_{n=1}^{N_p} \frac{c_n(z)}{j\lambda^2 - p_n(z)}, \tag{10}$$

is determined via the least squares-based fitting algorithm described in [15]. The coefficients p_n and c_n ($n = 1, \ldots, N_p$) are either real or come in complex conjugate pairs. Moreover, the p_n's are chosen so that $\mathrm{Re}[p_n]<0$, and as a consequence the contour $C_1 + C_2$ encloses the

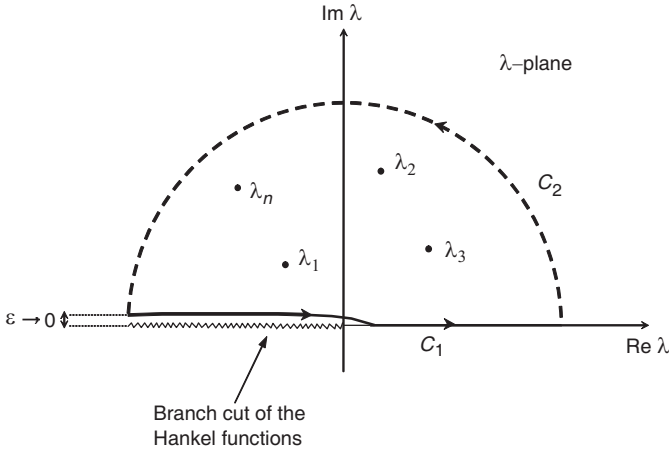

Figure 2. Closed path for the application of the residue theorem.

pole singularities $\lambda_n = \sqrt{-jp_n}$ $(n = 1, \ldots, N_p)$. Substitution of (10) into (9) and use of the residue theorem [20] lead to:

$$\overline{E}_\varphi(r,z) = 2j\overline{I}a \sum_{n=1}^{N_p} \Re_{\lambda_n}\left[b_n(\lambda,r,z)\right], \tag{11}$$

with

$$b_n(\lambda,r,z) = \frac{c_n(z)}{j\lambda^2 - p_n(z)}\, q(\lambda,r)\,\lambda, \tag{12}$$

and where

$$\Re_{\lambda_n}\left[b_n(\lambda,r,z)\right] = \lim_{\lambda\to\lambda_n}\left[(\lambda-\lambda_n)\, b_n(\lambda,r,z)\right] = \frac{1}{2j}\, c_n(z)\, q\left[\lambda_n(z),r\right] \tag{13}$$

is the residue of $b_n(\lambda,r,z)$ at $\lambda = \lambda_n$.

Finally, substituting (13) into (11) yields:

$$\overline{E}_\varphi(r,z,h) = \overline{I}a \sum_{n=1}^{N_p} c_n(z,h)\, q\left[\lambda_n(z,h),r,a\right], \tag{14}$$

where the dependences of the coefficients c_n and λ_n upon h and that of q upon the loop radius a are made explicit. Computational efforts of the proposed methodology are limited to the calculation of the c_n's and λ_n's, and the accuracy of the results depends only on the quality of

fitting. No expensive sample-domain optimization process is required, since the integral in (9) is solved analytically.

Closed-form expressions for the electric field distributions induced in tissues by multi-turn coils can be derived by superposing solutions of the form (14) valid for the separate turns. Coplanar turns share the same set of poles and residues and, as a consequence, electric field distributions arising from flat coils are computed with minimum time consumption. This is the case, for instance, of the pancake-shaped coil made up of N concentric turns having different radii varying from a_1 (inner radius) to a_N (outer radius). Summing up the contributions (14) from all the turns of the coil leads to

$$\overline{E}_{\varphi}^{(pc)}(r,z,h) = \overline{I}\sum_{i=1}^{N} a_i \sum_{n=1}^{N_p} c_n(z,h)\, q\left[\lambda_n(z,h), r, a_i\right]. \qquad (15)$$

Analogous expressions can be obtained for coils constituted by non-concentric turns. In these cases, the summation of the various contributions is performed after splitting the electric field vector generated by the i-th turn into its cartesian components along the x and y axes belonging to the coil plane (Fig. 3). From (14), it follows that:

$$\overline{E}_{x_i}(x,y,z,h) = -\frac{\overline{I}_i a_i (y-y_i)}{r_i} \sum_{n=1}^{N_p} c_n(z,h)\, q\left[\lambda_n(z,h), r_i, a_i\right], \quad (16)$$

$$\overline{E}_{y_i}(x,y,z,h) = \frac{\overline{I}_i a_i (x-x_i)}{r_i} \sum_{n=1}^{N_p} c_n(z,h)\, q\left[\lambda_n(z,h), r_i, a_i\right], \quad (17)$$

where $P_i \equiv (x_i, y_i)$ is the center of the i-th turn, and $r_i = \sqrt{(x-x_i)^2 + (y-y_i)^2}$. The total electric field components are expressed as:

$$\overline{E}_x(x,y,z,h) = \sum_{i=1}^{N} \overline{E}_{x_i}(x,y,z,h), \qquad (18)$$

$$\overline{E}_y(x,y,z,h) = \sum_{i=1}^{N} \overline{E}_{y_i}(x,y,z,h), \qquad (19)$$

Notice that all the feasible flat coil geometries placed at height h above the tissue correspond to a unique set of poles and residues. This feature is particularly useful when it is necessary to search for the optimum coil that produces a desired field pattern, since the

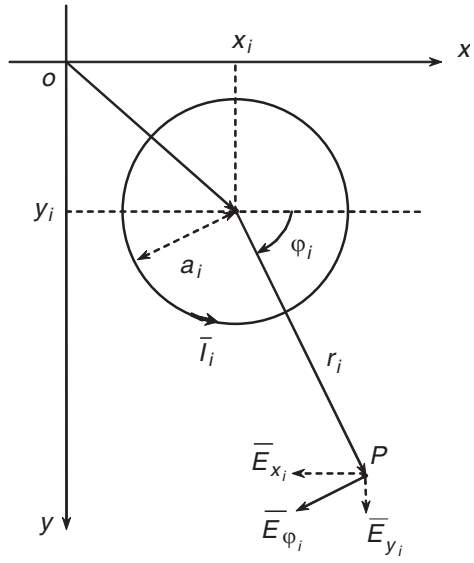

Figure 3. Geometry for the i-th turn.

conventional approach for solving such inverse problem relies on the computation of the patterns associated to coils of various shapes and sizes within an optimization loop. As the c_n's and λ_n's are calculated before entering the optimization algorithm, the computational work that remains to be done at each iteration is negligible. This alone makes the proposed methodology advantageous over purely numerical techniques like the finite difference time domain and finite element methods.

3. RESULTS AND DISCUSSION

3.1. Validation of the Method

Since therapeutic heating is required in deeper regions of human body, the developed theory is applied to the computation of the SAR induced in the muscle tissue sketched in Fig. 1 by a pancake round-shaped coil, which represents a widely used applicator for diathermy. The SAR (W/kg) in the muscle tissue is expressed as:

$$\mathrm{SAR}\,(r,z) = \frac{\sigma_2 E_\varphi^2(r,z)}{\rho_2}, \quad z > d, \tag{20}$$

where $\overline{E}_\varphi(r,z)$ is given by (15). The calculations are performed assuming $\sigma_1 = 0.033\,\mathrm{S/m}$, $\epsilon_{r_1} = 8.45$, $\rho_1 = 0.96\,\mathrm{g/cm^3}$, $\sigma_2 = 0.71\,\mathrm{S/m}$, $\epsilon_{r_2} = 91.6$, and $\rho_2 = 1.02\,\mathrm{g/cm^3}$ [21]. The coil has four compactly wound turns, inner radius $a_1 = 5.4\,\mathrm{cm}$ and outer radius $a_4 = 6\,\mathrm{cm}$. The wire, 0.2 cm in diameter, carries a current of 1 A. The coil-to-subject spacing and fat layer thickness are respectively $h = 3.5\,\mathrm{cm}$ and $d = 2.25\,\mathrm{cm}$. At first, the distribution of the SAR is evaluated at depth $z' = z - d = 3.5\,\mathrm{cm}$ below the fat-muscle interface and at the frequency of 27.12 MHz. The obtained results, depicted in Figs. 4 and 5, show that the maximum of the deposited power is not on the axis of symmetry of the coil and is not restricted to a small region, but it is spread circularly under the edge of the coil.

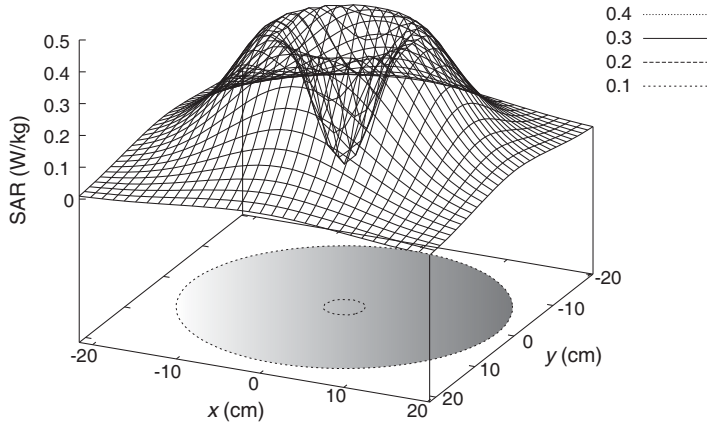

Figure 4. 3D view of the SAR distribution induced by the round coil in the muscle tissue 3.5 cm below the fat-muscle interface.

Figure 5 also illustrates the comparison among the SAR values obtained by applying (15) and those provided by the zero-order quasistatic model [10–13] and the FDTD method. Results achieved with the proposed high-order solution agree well with the FDTD data. On the contrary, the plotted curves demonstrate how the quasi-static assumption leads to overestimating the EM energy absorption, and this is a consequence of ignoring the attenuation of the electric field strength due to the depth of penetration. The absolute error generated by the zero-order model increases with the radial distance from the coil axis, up to the maximum value of 78 mW/kg at $r \cong 12\,\mathrm{cm}$ (Fig. 6). Thereinafter, the absolute error diminishes indefinitely.

As far as the relative error is concerned, it increases as the radial distance increases, with values comprised between 10% and 50% in the range $r = 3$–$17\,\mathrm{cm}$, where heating is at least one-third the peak value.

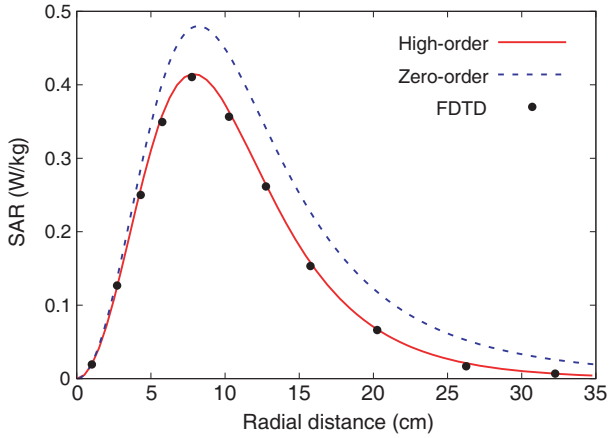

Figure 5. Radial distribution of the SAR induced by the round coil in the muscle tissue 3.5 cm below the fat-muscle interface.

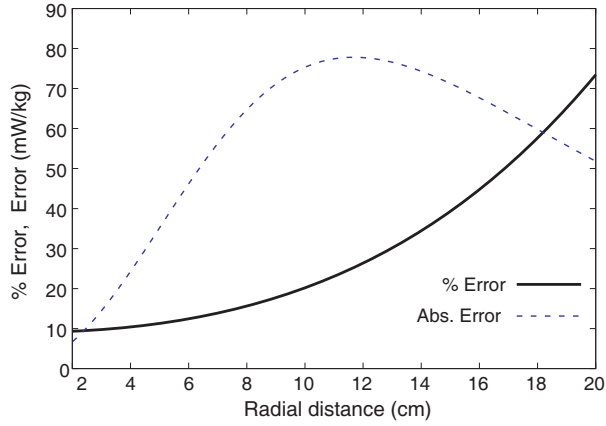

Figure 6. Radial distribution of the relative and absolute errors resulting from the SAR calculated by applying the zero-order approach.

For $r > 17$ cm, the relative error is greater than 50%, but has little relevance because of the poor heating.

Notice that fifty poles have been used for fitting the function (2). The fitting process has taken about 8 seconds on a 1.6 GHz PC, and the generated root-mean-square relative error is less than 10^{-13}. The real and imaginary parts of $f(\lambda, z)$ and the corresponding rational approximations are shown in Fig. 7.

It should be observed that the above analysis is referred to the

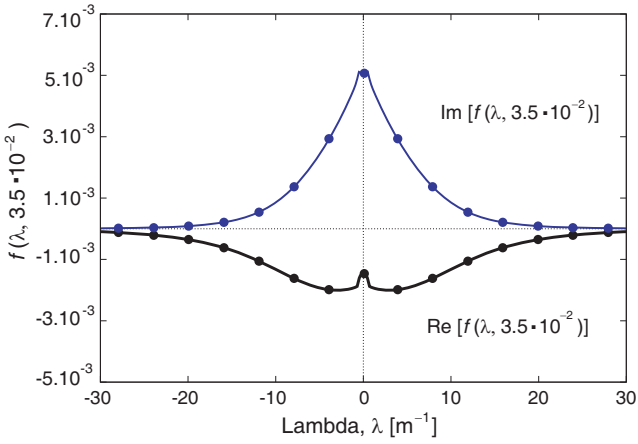

Figure 7. Real and imaginary parts of the function $f(\lambda, z)$ versus λ. Exact $(-)$ and rational approximation $(\bullet)$.

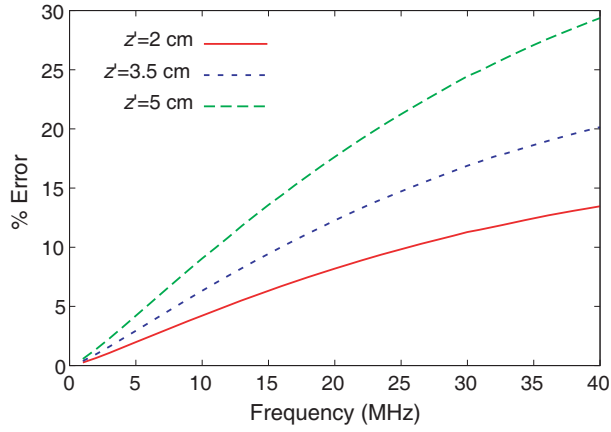

Figure 8. Relative percent error resulting from computing the peak heating by applying the zero-order model against frequency.

particular operating frequency of 27.12 MHz, and to the depth of $z' = 3.5$ cm from the muscle layer upper boundary.

At higher operating frequencies or deeper observation points the effective electric field amplitude is even more reduced with respect to that evaluated ignoring the depth of penetration. This aspect is pointed out in Fig. 8, where the relative error that results from computing the peak heating by applying the zero-order model rather

than the proposed one is plotted against frequency. The plotted curves show that at the frequency of 1 MHz and lower the relative error produced by the zero-order model is almost null for every depth z' of the observation point in the muscle tissue. In fact, at 1 MHz the values of depth of penetration in fat and muscle are large if compared respectively to the thickness of the fat layer and the depth of the observation point from the muscle upper boundary, and the total and the incident electric fields are substantially coincident. Thereinafter, the relative percent error grows up with increasing frequency and, for the same frequency, higher errors are generated at deeper locations. At 40.68 MHz and for $z' \geq 5$ cm the relative percent error exceeds 30%.

3.2. Figure-eight Geometry

As a special case of multiple-coil configuration, the figure-eight or butterfly-shaped coil is considered in this paragraph. This geometry consists of a coplanar pair of oppositely connected round coils (see Fig. 9), and produces a localization of the deposited power under the point of intersection, where the eddy current densities induced by the two coils are additive.

The SAR deposited in the muscle tissue is expressed as:

$$\mathrm{SAR} = \frac{\sigma_2 \left(E_x^2 + E_y^2\right)}{\rho_2}, \tag{21}$$

where $\overline{E}_x$ and $\overline{E}_y$ are given by (18) and (19). The SAR is computed

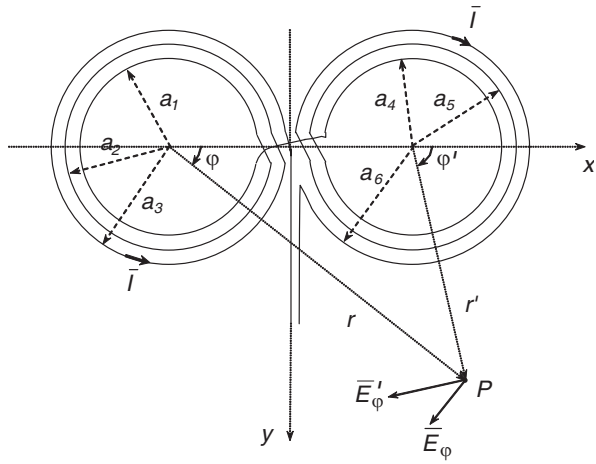

Figure 9. Geometry and coordinates for a figure-eight coil.

at depth $z' = 3.5\,\text{cm}$ from the fat-muscle boundary, assuming that the coil has six turns, with $a_1 = a_4 = 2\,\text{cm}$, $a_2 = a_5 = 2.2\,\text{cm}$, and $a_3 = a_6 = 2.4\,\text{cm}$, and carries a current $\overline{I} = 3\,\text{A}$ at 27.12 MHz. Notice that the electric field components (18) and (19) are calculated by using the same set of poles and residues found for the single round coil. Numerical results are shown in Figs. 10 and 11, which present, respectively, a 3D view and the profile along the x-axis of the absorbed

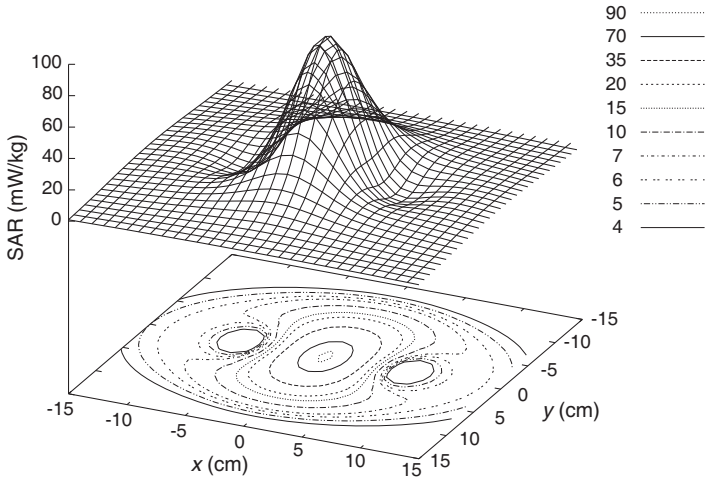

Figure 10. 3D view of the SAR distribution induced by the butterfly coil in the muscle tissue 3.5 cm below the fat-muscle interface.

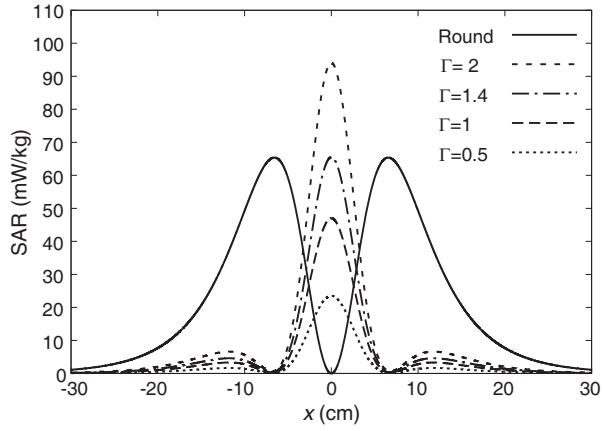

Figure 11. Computed SAR profiles along the x-axis. Round (solid line) and butterfly (dashed lines) coils.

power density.

Figure 11 illustrates the SAR profiles arising from both the butterfly coil (upper dashed line) and its left wing alone centered at the origin of the x-y plane (solid line). From the comparison between these two curves it turns out that closing together two round N-turn coils to form a butterfly geometry increases the peak heating. This is made at the cost of doubling the required Joulean and magnetic field energies. In fact, if the total resistance and self-inductance are, respectively, R_B and L_B for the butterfly coil with $2N$ turns, R_W and L_W for the single wing with N turns, it results [11]:

$$R_B(2N) = 2R_W(N), \quad L_B(2N) \cong 2L_W(N), \tag{22}$$

and, consequently,

$$P_B(2N, I) = R_B(2N)I^2 = 2R_W(N)I^2 = 2P_W(N, I), \tag{23}$$

$$U_B(2N, I) = L_B(2N)I^2 \cong 2L_W(N)I^2 = 2U_W(N, I), \tag{24}$$

where $P = RI^2$ is the average power dissipated by R, and $U = LI^2$ is the energy in the magnetic field when the current in the coil is maximum ($I_{\max} = I\sqrt{2}$). In order to discern whether the butterfly coil is more efficient than the single wing or not, comparison should be made between the heating patterns generated from the same amount of energy. For this purpose, the values $2N'$ and I' for the number of turns and the current in the butterfly coil are determined that make the required active power $P_B(2N', I')$ and magnetic energy $U_B(2N', I')$ equal respectively to $P_W(N, I)$ and $U_W(N, I)$. The system of equations to be solved is the following

$$2R_W(N'){I'}^2 = R_W(N)I^2, \tag{25}$$

$$2L_W(N'){I'}^2 = L_W(N)I^2, \tag{26}$$

and can be further reduced to one equation by introducing the well-known expressions for the resistance and self-inductance of a round coil [11]

$$R_W(N) = \alpha_R N^2, \quad L_W(N) = \alpha_L N^2, \tag{27}$$

where α_R and α_L depend on geometrical factors (i.e., the inner and outer radii). It yields:

$$2N'^2 I'^2 = N^2 I^2, \tag{28}$$

that is, for fixed N and I, the equation of an equilateral hyperbola. Notice that the function

$$\Gamma(N', I') = \frac{P_B(2N', I')}{P_W(N, I)} = \frac{U_B(2N', I')}{U_W(N, I)} = 2\left(\frac{N'I'}{NI}\right)^2, \tag{29}$$

which represents the normalized dissipated power as well as the normalized maximum magnetic energy in the butterfly coil, is constantly equal to unity when moving along such hyperbola. Hence, Equation (28) describes a level curve (contour line) of Γ.

It can be numerically verified that all the points (N', I') belonging to a contour line (hyperbola) of Γ lead to the same heating pattern. For instance, the SAR profile of Fig. 11 corresponding to $\Gamma = 2$ is obtained either assuming $(N', I') = (N, I) = (3, 3\,\mathrm{A})$, as it has been made, or for any other choice of N' and I' such that $N'I' = NI = 9\,\mathrm{A}$.

From the analysis of the curve labeled with $\Gamma = 1$ it can be concluded that, when the provided energy is the same for the two configurations, the peak heating produced by the butterfly coil is about one-fourth lower than that generated by the round one. Furthermore, contrarily to what has been argued in previous works [10, 11], the curve indicated with $\Gamma = 1.4$ demonstrates that both the Joulean and magnetic energies required to induce a given SAR intensity with a two-coil geometry are larger (by 40 percent) than and not about half those required with a single round coil of the same inner and outer radii as each of the two coils.

In fact, for $\Gamma = 0.5$ (that is for $N' = N = 3$ and $I' = I/2 = 1.5\,\mathrm{A}$), the maximum power density deposited by the butterfly coil is 23.5 mW/kg. The round coil provides this value of SAR, which is significantly less than the maximum, at radial distance $r = 2.4\,\mathrm{cm}$ from the axis, that is at a point approximately under the coil edge (located at $r = 2.6\,\mathrm{cm}$). It is true that, after halving the energy supply, the SAR calculated under the edge of a round coil does not change if it is joined to another coil with identical dimensions. At the same time, it is also true that the peak SAR diminishes by a factor of 3 (see Fig. 11). Despite of increasing electric field focality, the butterfly geometry is less energetically efficient than the single coil geometry. It has been pointed out that the computational cost of the proposed approach is significantly smaller than that implied by numerical techniques like the FDTD method, whenever it is required to optimize the coil to produce a prescribed heating pattern. However, this advantage might be lost if the coil geometries that are going to be considered within the optimization loop are not composed of circular turns. For such more complicated sources, the FDTD method is then a more flexible and standardized technique. Finally, it should be observed that the energetic efficiency as well as the degree of localization (i.e. the focality) of diathermy treatment can be directly deduced from the spatial distribution of the power density deposited in the tissue. The temperature rise in the tumor or treated area, instead, cannot be quantified on the basis of the SAR alone, since it is heavily determined

by the blood flow in local vessels. In fact, the increase in blood flow due to vasodilatation has a cooling effect. Even the effectiveness of the treatment does not depend uniquely on the SAR distribution induced by the coil, as it varies also according to the patient pain tolerance.

4. CONCLUSION

A method has been developed that allows to determine a high-order closed-form solution for the SAR distribution induced inside a fat-muscle tissue by a diathermy induction coil. The method has been derived starting from the exact complete expressions for the EM field components generated by a current-carrying circular loop placed above a stratified earth. The integral expression describing the elementary contribution of the generic turn of the coil to the total produced electric field is integrated according to an exact procedure, once the non-oscillating part of the integrand is replaced with an accurate rational approximation generated by a fitting algorithm. The process of integration takes only few seconds, since the computational effort is limited to the extraction of the poles and residues of the rational approximation. The obtained closed-form solution is valid in a wide frequency range, and is different from the commonly used zero-order formulations that do not account for the attenuation of the electric field magnitude in the tissue due to the depth of penetration.

In the case of flat multi-turn coils, the heating patterns induced in tissues are computed by superposing the simple solutions valid for the separate turns. Since the poles and residues to be determined are the same for all the coplanar turns which constitute the coil, time consumption is minimum and is only weakly affected by the number of turns and the shape of the coil. Furthermore, the poles and residues obtained for a particular coil geometry can be used for analyzing the performances of an infinite number of coplanar geometries, with clear advantages in terms of computational cost. This alone makes the proposed methodology exceptionally useful when it is necessary to search for the optimum coil that produces a desired field pattern, and convenient with respect to any purely numerical technique commonly used to solve electromagnetic boundary value problems, like the FDTD or finite element methods. Spatial distributions of the SAR induced in muscle tissue by round and figure-eight coils are computed by applying the developed method. The obtained results are in excellent agreement with those provided by FDTD simulations. Conversely, the observed disagreement with numerical data produced by the zero-order model confirms that the quasi-static expressions for the field components lead to overestimating the EM energy absorption, and this is a consequence

of ignoring the high-frequency effects of the depth of penetration in the tissue. Finally, the investigation of the heating pattern of a figure-eight coil has allowed to conclude that, surprisingly, such geometry is less efficient than the round one, though doubtless capable of producing a more localized electromagnetic field.

REFERENCES

1. Hill, J., M. Lewis, P. Mills, and C. Kielty, "Pulsed short-wave diathermy effects on human fibroblast proliferation," *Arch. Phys. Med. Rehabil.*, Vol. 83, No. 6, 832–836, 2002.
2. Santoro, D., L. Ostrander, B. Y. Lee, and B. Cagir, "Inductive 27.12 MHz diathermy in arterial peripheral vascular disease," *EMBS 1994, Proc. IEEE 16th Annual Intern. Conf.*, Vol. 2, 776–777, 1994.
3. Guy, A. W., J. F. Lehmann, and J. B. Stonebridge, "Therapeutic applications of electromagnetic power," *Proceedings of the IEEE*, Vol. 62, No. 1, 55–75, 1974.
4. Rhattoy, A., S. Bri, and M. Audhuy-Peudecedery, "Coaxial antenna for microwave hyperthermia," *Journal of Electromagnetic Waves and Applications*, Vol. 19, No. 14, 1963–1971, 2005.
5. Rajhi, A., "Optimization of the EM heating cycle by using a dual frequency local hyperthermia applicator," *Journal of Electromagnetic Waves and Applications*, Vol. 17, No. 3, 447–464, 2003.
6. Wu, M. S., K. Ito, and H. F. Kasai, "Analysis of current and electric field distributions of coaxial-slot antenna for interstitial microwave hyperthermia," *Journal of Electromagnetic Waves and Applications*, Vol. 9, No. 5–6, 831–849, 1995.
7. Kerem, M. and K. Yigiter, "Effects of continuous and pulsed shortwave diathermy in low back pain," *The Pain Clinic*, Vol. 14, No. 1, 55–59, 2002.
8. Sciuto, M. G., C. Zanon, A. Mussa, R. Clara, M. Bortolini, A. Malossi, R. Moscato, P. Celoria, M. De Andrea, M. Rizzo, and I. Chiappino, "Chemohyperthermia for advanced abdominal malignancies: A new procedure with closed abdomen and previously performed anastomosis," *International Journal of Hyperthermia*, Vol. 17, No. 5, 456–464, 2001.
9. Curto, S. and M. J. Ammann, "Electromagnetic coupling mechanism in a layered human tissue model as reference for 434 MHz RF medical therapy applicators," *Proc. 2007 IEEE*

Antennas and Propagation Society International Symposium, Vol. 1, 3185–3188, 2007.

10. Ren, C., P. P. Tarjan, and D. B. Popovic, "A novel electric design for electromagnetic stimulation — The slinky coil," *IEEE Trans. Biomed. Eng.*, Vol. 42, No. 9, 918–925, 1995.
11. Nyenhuis, J. A., G. A. Mouchawar, J. D. Bourland, and L. A. Geddes, "Energy considerations in the magnetic (Eddycurrent) stimulation of tissues," *IEEE Trans. Magnetics*, Vol. 27, No. 1, 680–687, 1991.
12. Esselle, K. P. and M. A. Stuchly, "Quasi-static electric field in a cylindrical volume conductor induced by external coils," *IEEE Trans. Biomed. Eng.*, Vol. 41, No. 2, 151–158, 1994.
13. Schnabel, V. and J. J. Struijk, "Calculation of electric fields in a multiple cylindrical volume conductor induced by magnetic coils," *IEEE Trans. Biomed. Eng.*, Vol. 48, No. 1, 78–86, 2001.
14. Singh, N. P. and T. Mogi, "Electromagnetic response of a large circular loop source on a layered earth: A new computation method," *Pure and Applied Geophysics*, Vol. 162, No. 1, 181–200, 2005.
15. Gustavsen, B. and A. Semlyen, "Rational approximation of frequency domain responses by vector fitting," *IEEE Trans. Power Delivery*, Vol. 14, No. 3, 1052–1061, 1999.
16. Cristina, S. and M. Parise, "Closed-form expression of the SAR distribution in a multilayered planar model for shortwave inductive diathermy," *Proc. IEEE 1st Intern. Conf. Bio. Medical Engineering & Informatics*, Vol. 2, 577–582, 2008.
17. Guptasarma, D. and B. Singh, "New digital linear filters fo Hankel J0 and J1 transforms," *Geophysical Prospecting*, Vol. 45, No. 5, 745–762, 1997.
18. Kong, F. N., "Hankel transform filters for dipole antenna radiation in a conductive medium," *Geophysical Prospecting*, Vol. 55, No. 1, 83–89, 2007.
19. Felsen, L. B. and N. Marcuvitz, *Radiation and Scattering of Waves*, IEEE Press, Piscataway, NJ, 1994.
20. Marsden, J. E. and M. J. Hoffman, *Basic Complex Analysis*, W. H. Freeman and Company, New York, 1998.
21. "Tissue dielectric properties," Federal Communications Commission, Washington, DC [Online], http://www.fcc.gov/fcc-bin/dielec.sh.